Journal of
Composites Science

MDPI

Article

Platinum-Decorated TiO_2: One Step Fast Monometallic Impregnation and Plasma Effect on Nanoparticles

Rudy Trejo-Tzab [1,*], Alejandro Avila-Ortega [1], Patricia Quintana-Owen [2], Ricardo Rangel [3] and Mayra Angélica Álvarez-Lemus [4]

[1] Facultad de Ingeniería Química, Universidad Autónoma de Yucatán, Merida C.P. 97203, Yucatán, Mexico; alejandro.avila@correo.uady.mx
[2] Departamento de Física Aplicada, CINVESTAV-Unidad Mérida, A.P. 73, Cordemex, Merida C.P. 97310, Yucatán, Mexico; pquint@cinvestav.mx
[3] Facultad de Ingeniería Química, Universidad Michoacana de S. N. H., Morelia C.P. 58060, Michoacán, Mexico; rrangel@umich.mx
[4] Laboratorio de Nanotecnología, División Académica de Ingeniería y Arquitectura, Universidad Juárez Autónoma de Tabasco, Cunduacan 86690, Tabasco, Mexico; mayra.alvarez@ujat.mx
* Correspondence: rudy.trejo@correo.uady.mx

Abstract: In the present work, N-TiO_{2-x}/Pt was synthesized using a homemade nitrogen plasma (AC) discharge system. The overall procedure use of low-power nitrogen plasma (100 watts) with 1 and 2 h of plasma discharge to successfully impregnate platinum nanoparticles on P25 titanium dioxide. The obtained samples were characterized using X-ray diffraction (XRD), UV–Vis diffuse reflectance spectroscopy (DRS), X-ray photoelectron spectroscopy (XPS), and high-resolution transmission electron microscopy (HRTEM). The results reveal the incorporation of metallic Pt up to 2.9% on the surface of TiO_2 by increasing the duration of plasma discharge by up to two hours with a constant power of 100 watts. Likewise, the incorporation of nitrogen atoms into a lattice crystal was also favored, confirming a direct relationship between the amount of Pt and nitrogen atoms introduced in TiO_2 as a function of the duration of plasma treatment. By characterizing nanoparticles loaded on a N-TiO_{2-x}/Pt surface, we show that joined platinum nanoparticles have two different patterns, and the boundary between these two regions coalesces. The results demonstrate that the use of nitrogen plasma to impregnate platinum nanoparticles on the surface of TiO_2 to obtain N-TiO_{2-x}/Pt allows wide and relevant physics and chemistry applications.

Keywords: plasma; nanoparticles; metal-decorated; N-doped TiO_2; chemical deposition

Citation: Trejo-Tzab, R.; Avila-Ortega, A.; Quintana-Owen, P.; Rangel, R.; Álvarez-Lemus, M.A. Platinum-Decorated TiO_2: One Step Fast Monometallic Impregnation and Plasma Effect on Nanoparticles. *J. Compos. Sci.* **2022**, *6*, 4. https://doi.org/10.3390/jcs6010004

Academic Editors: Konda Gokuldoss Prashanth and Francesco Tornabene

Received: 24 November 2021
Accepted: 20 December 2021
Published: 24 December 2021

1. Introduction

In recent decades, due to the optical properties, chemical stability, and great oxidizing potential of catalysts based on TiO_2, numerous studies have been carried out regarding the production of these materials [1–5]. Their photocatalytic properties have successfully enabled the elimination of pollutants in water flows and air [6–8] through reactions induced by photogenerated electron–hole pairs occurring on the TiO_2 semiconductor surface [9]. Such capabilities have generated great interest in TiO_2 compounds. However, because the absorption range of TiO_2 is restricted to the UV region of the electromagnetic spectrum, the photonic efficiency of this material is less than ~10% [10]. To improve the activity and photocatalytic performance of TiO_2, different strategies have been used, such as nonmetallic doping (especially with nitrogen) and transition metal impregnation, including Au, Ag, Cu, and Pt, on the titanium dioxide surface, which act as photogenerated electron traps [3]. The methodologies that have been used for metal impregnation on TiO_2 are varied, which are also dependent on the metal to be impregnated. For instance, chemical deposition and liquid impregnation have been successfully applied to deposit silver (Ag-NPs) or platinum nanoparticles (Pt-NPs) using $AgNO_3$ and H_2PtCl_6 compounds as metal precursors, respectively [11–13]. In another study, a postdeposition method was used to obtain TiO_2/Au by impregnating gold nanoparticles (Au-NPs) from a colloidal solution of Au using $HAuCl_4$ as

a metal precursor [14]. Likewise, the flame spray pyrolysis process (FSP) has demonstrated its versatility for incorporating monovalent fluoride into the crystalline lattice of titanium oxide in the production of F-doped TiO_2/Pt. In this case, hydrated hexachloroplatinic acid was used as a precursor of platinum metal, and hexafluorobenzene was used as a fluorine precursor [15]. It is noteworthy that investigations using chemical processes for metal impregnation have made great progress; the excellent and promising results demonstrate the good synergy of these metals with titanium oxide. Thus, the metal–titania relationship has opened new areas of research in photocatalysis.

On the other hand, platinum is one of the most promising and active metals for increasing the photocatalytic efficiency of TiO_2 because it produces the highest Schottky barrier to facilitate the electrons capture, and therefore the electron–hole pair recombination rate decreases [16]. Pt-TiO_2 has been used in many photocatalytic reactions under visible light irradiation, for example, in the degradation of Rhodamine B, photocatalytic oxidation of formaldehyde and glycerol [17–19]. Similarly, Pt-TiO_2 was used for the oxidation-reduction of benzoic acid [20] and in the degradation of different azo dyes, such as amaranth, sunset yellow, and tartrazine [13], as well as in redox reactions such as water splitting for the generation of hydrogen [21]. Pt-TiO_2 has been achieved mainly by chemical processes, including the Flame Spray Pyrolysis process (FSP). In this work, we discuss the preparation of Pt-TiO_2 applying nitrogen plasma where titanium powder is exposed to the nitrogen plasma to obtain N-TiO_{2-x}/Pt powder photocatalysts.

In a previous work, it has been demonstrated that argon and nitrogen plasma synthesis methods have yielded good results for the impregnation of gold and copper particles on titanium oxide [22,23]. Moreover, this approach has proven to be an effective and environmentally friendly technology due to the rapid production of compounds without the generation of chemical byproducts. This new methodology has also been used with great success to induce phase changes in titanium oxide from amorphous TiO_2 [24], and to the best of our knowledge, Pt impregnation on semiconductor materials applying nitrogen plasma are scarce. Taking advantage of the previous experience of our research group, we explored the feasibility of producing N-TiO_{2-x}/Pt in a single stage by studying the effect of nitrogen plasma to promote Pt metal impregnation and nitrogen doping. The characterization of the catalysts obtained through the XRD, XPS, and DRS studies are presented.

2. Materials and Methods

2.1. Materials

Degussa P25 titanium oxide (Evonik Ind. AG) and a metal foil of platinum (Pt) with a thickness of 0.025 mm and 99.9% purity (Sigma-Aldrich) were used. The used working gas was nitrogen with 99.99% purity (Praxair). The methodology for platinum monometallic impregnation was already reported by R. Trejo-Tzab et al. [22,23], which consists of covering the lower electrode with the metal to be impregnated: in this case, Pt foil. Therefore, titanium oxide P25 (200 mg) was dispersed on the Pt foil. A diffusion pump LABCONCO (Mod 195 A65412906) was used to evacuate the plasma chamber and to maintain a working pressure of 8.5×10^{-2} Torr. A nitrogen flow inside the plasma reactor was kept at constant pressure, while a discharge was applied between electrodes, producing nitrogen plasma inside the reactor using a power of 100 watts. The sample was analyzed after 1 and 2 h of plasma discharge in a "batch" process. However, after one hour, it was mechanically homogenized in an agate mortar. Thus, N-TiO_{2-x}/Pt samples were obtained; the experimental setup is shown in Figure 1.

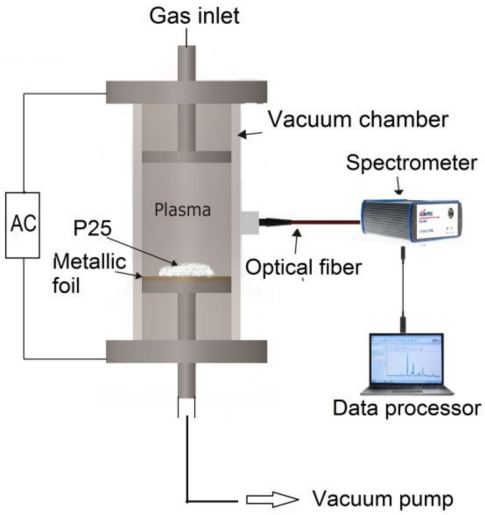

Figure 1. Schematic arrangement of the plasma system.

2.2. Characterization

Optical emission spectroscopy (OES) was used to follow up the emission of the nitrogen plasma at all times during the plasma treatment. The studies were performed with a Starline UV–Vis spectrophotometer (AvaSpec-3648, Avantes, Apeldoorn, The Netherlands). The crystal structure of the samples was analyzed using X-ray diffraction (XRD, Bruker D8 Advance, Billerica, MA, USA) with a Cu kα source (1.5418 Å wavelength, operating at 30 mA). The patterns were recorded in a 2θ interval from 10 to 90°, and the diffraction patterns were analyzed using the ICDD database (International Center for Diffraction Data, PDF2016). The surface composition and chemical valence of samples was determined by X-ray photoelectron spectroscopy (XPS) (Thermo Fisher Scientific K-alpha system with a Kα source, 1400 eV, Waltham, MA, USA). The energy values were calibrated considering the C 1s signal (284.6 eV). All samples were pretreated during 15 s with argon to exclude surface impurities. The XPS equipment uses an internal standard to correct charge variations. Diffuse reflectance spectroscopy (DRS) studies were performed to determine the energy bandgap changes in the samples after the plasma treatments. The UV–Vis diffuse reflectance spectra were obtained with a Starline spectrophotometer model AvaSpec-3648 equipped with an integration sphere (AvaSphere-50-REFL, Apeldoorn, The Netherlands) and a UV–Vis deuterium–halogen light source (AvaLight DH-S-BAL, Avantes, Apeldoorn, The Netherlands). The shape and particle size were determined by high-resolution transmission electron microscopy, HRTEM (JEOL, Mod. JEM 2100 operating at 200 kV, Tokyo, Japan).

3. Results and Discussion

3.1. Optical Emission Spectroscopy (OES)

Figure 2 shows the optical emission spectral data of N_2 plasma. The peaks with the highest emission intensities, located at 337 nm and 391.1 nm, are due to emission produced by radiative decay corresponding to the N_2 molecule and N_2^+ ion emission, respectively. The electronic state population observed for N_2, as well as that for the N_2^+ ion, is mainly due to direct excitation of N_2 and N_2^+ from their ground state, produced by impacting electrons having energies above their excitation threshold. In the emission spectrum, the intensity of both peaks is proportional to the electron density of N_2 and N_2^+. The obtained emission spectra are in agreement with previous studies carried out by other research groups, for instance, Qayyum et al. and Abdel-Fattah et al., who reported emission peaks similar to those found in the present work [25,26].

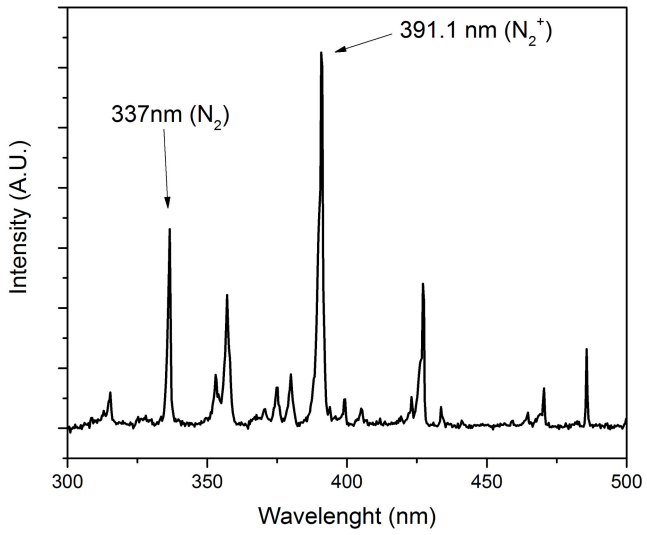

Figure 2. Emission spectrum for nitrogen plasma.

3.2. X-ray Diffraction (XRD)

Quantitative analyses of the crystalline phases in the samples, that is to say, the weight fractions of anatase (%wt_A) and rutile (%wt_R), were determined by means of Spurr–Meyer's method applying the following equation [27]:

$$\%wt_A = \frac{1}{1 + 1.265\left(\frac{I_R}{I_A}\right)} \times 100 \quad (1)$$

$$\%wt_R = 100 - \%wt_A \quad (2)$$

where I_A and I_R correspond to the integrated intensities of anatase (101) and (110) rutile reflections. The same XRD reflections were also used to calculate the average crystallite sizes applying the Scherrer equation:

$$L = \frac{0.9\lambda}{\beta \cos\theta} \quad (3)$$

where L is the crystal size and corresponds to the average value of the volume-weighted particle size distribution, λ is the wavelength of the X-rays, β is the full width in radians subtended by the half-maximum intensity width of the powder pattern peak which is the observed FWHM, and θ is the Bragg angle.

XRD analyses of the monometallic TiO_2/Pt sample obtained after 1 h and 2 h (Figure 3) show that the intensity of the main peaks of anatase (101) and rutile (110) do not present significant changes after having been subjected to the nitrogen plasma. Likewise, they show that the crystallinity of P25 TiO_2 does not change after the plasma treatments. This means that their composition ratio confirmed using the Spurr–Meyer's equations remains constant in a range of 70% anatase and 30% rutile. On the other hand, the average crystalline domain size of pure P25 TiO_2 was calculated from the Scherrer equation with a crystallite size of about 26 ± 3 nm, and no significant changes in crystalline size after plasma treatment were found. Furthermore, through the XRD analysis shown in Figure 3, we can see the characteristic (111), (200), and (220) diffraction peaks of platinum, which are observed at 39.7°, 46.0°, and 67.3° (2θ) values, respectively. These peaks are more intense for the samples subjected to 120 min of treatment. The insets located in Figure 3a,b show a deconvolution analysis carried out in the samples, where an additional diffraction peak was observed at 39.70° (2θ) and was indexed to the (111) plane corresponding to metallic Pt. The intensity of this peak was stronger after 2 h of plasma treatment than that obtained for 1 h, confirming that nitrogen plasma promotes the impregnation of Pt particles on

the titanium oxide surface. Likewise, the intensity of (200) and (220) diffraction planes corresponding to Pt were more evident in the XRD pattern after 2 h of plasma processing.

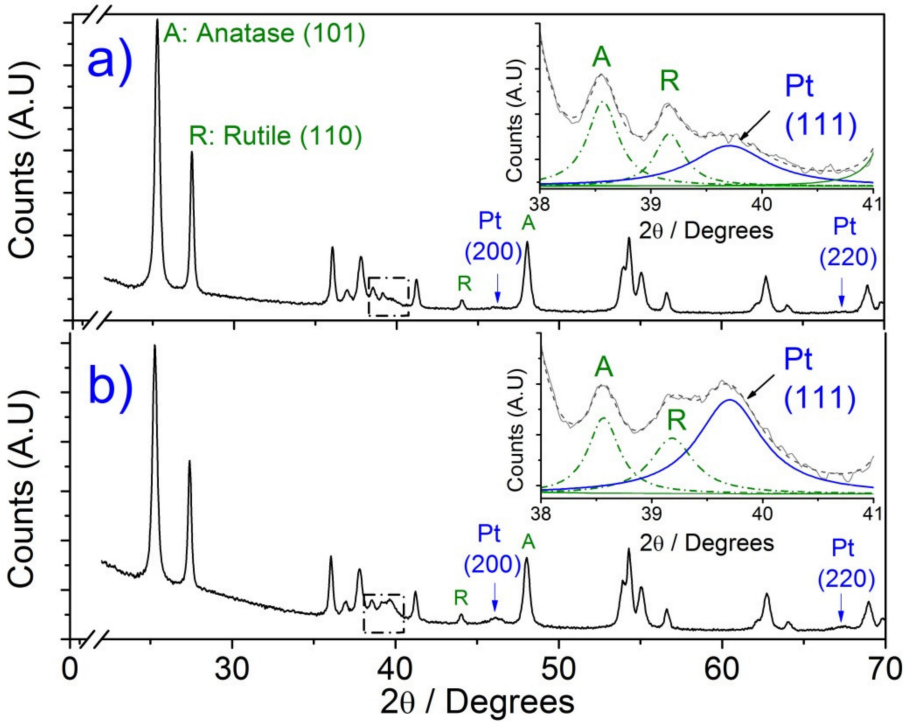

Figure 3. XRD diffraction pattern of the monometallic samples obtained at (**a**) 1 h and (**b**) 2 h treatment times with nitrogen plasma (A: anatase, R: rutile, Pt: platinum).

3.3. X-ray Photoelectron Spectroscopy (XPS)

X-ray photoelectron spectroscopy (XPS) was used to analyze the chemical states of the elements in samples obtained after plasma treatments. The XPS spectra of Ti 2P are shown in Figure 4 and exhibit the characteristic Ti 2P binding energies, labeled as Ti $2P_{3/2}$ and Ti $2P_{1/2}$ doublets, which are associated with the Ti^{4+} valence state on oxygen lattice. A binding energy shift can be observed in N-TiO_{2-x}/Pt sample after 2 h nitrogen plasma treatment compared to the standard TiO_2; however, no shifting was observed for C 1s peak position (see inset in Figure 4). An important variation in the position of the band attributable to Ti(IV) in the Ti-O bond can be observed, when compared to the TiO_2 spectrum. The shift to a lower binding energy of Ti $2P_{3/2}$ detected for N-TiO_{2-x}/Pt can be caused by nitrogen doping, as shown in the N 1s XPS spectra (Figure 5b). This observation has been confirmed by other research groups who correlate the shift to a lower binding energy with substitutional and interstitial nitrogen atoms into the TiO_2 matrix [28].

On the other hand, the characteristic signals of platinum can be seen in Figure 5a. The Pt 4f binding energies are observed at 70.68 eV (Pt $4f_{7/2}$) and 74.03 eV (Pt $4f_{5/2}$) and are ascribed to metallic platinum (Pt^0). Moreover, it shows an additional two peaks at 71.16 eV (Pt $4f_{7/2}$) and 75.30 eV (Pt $4f_{5/2}$), which suggests the presence of platinum in its Pt^{2+} oxidation state, which means that PtO is also observed on the TiO_2 surface, and in this study, PtO_2 was not observed. However, in the XRD analyses (Figure 3), platinum oxide phase was not observed, and they only show metallic platinum (Pt) and titanium oxide phases; it is likely that the platinum oxide concentration is outside the equipment detection limit. These results agree with those of other studies carried out by different research groups that have applied chemical methods for incorporating platinum onto a TiO_2 surface; they report the presence of metallic platinum and platinum oxide on the material [20,29,30].

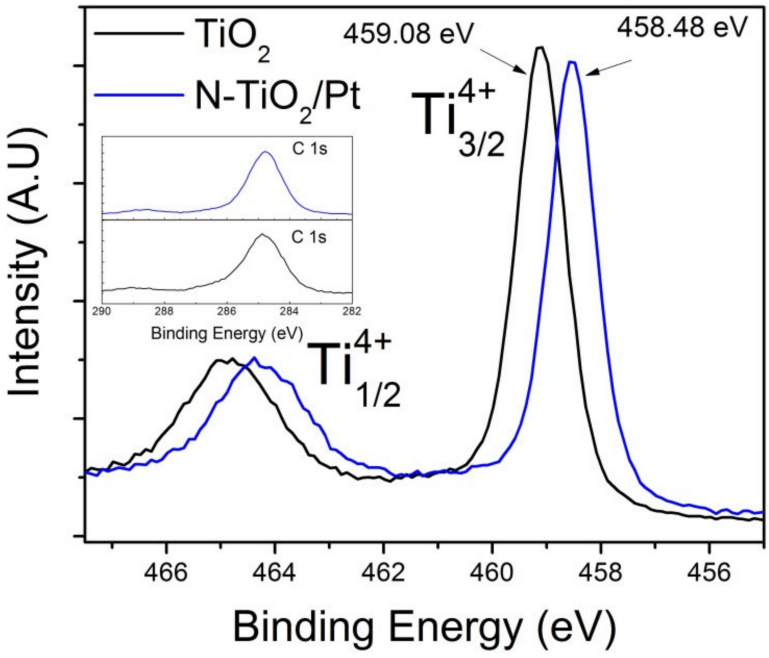

Figure 4. XPS spectra in the Ti2p region for TiO_2 and N-TiO_{2-x} /Pt (2 h nitrogen plasma treatment).

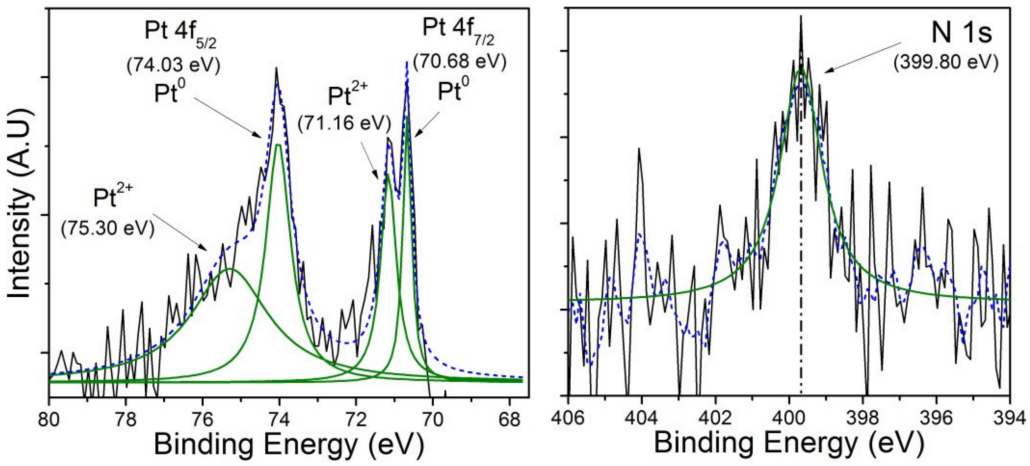

(**a**) (**b**)

Figure 5. XPS spectra of the sample N-TiO_{2-x} /Pt after 2 h nitrogen plasma treatment: (**a**) Pt and (**b**) nitrogen.

Figure 5b shows the nitrogen N 1s XPS spectrum, and a signal at 399.8 eV was observed. Viswanathan and Krishanmurthy et al. [31] attribute this signal to nitrogen occupying an interstitial site with a Ti-O-N bond in TiO_2 doped with nitrogen. This signal has been confirmed elsewhere, in which it is mentioned that a peak detected in the range from 396 to 404 eV indicates the replacement of oxygen by nitrogen atoms to form N-Ti-O and Ti-N-O bonds [20,31]. Valentin et al. propose that both substitutional and interstitial doping generate changes in the UV and UV–Vis optical properties of titania, which are related to the improvement of catalytic processes [32]. Due to the observed presence of Pt on the TiO_2 surface and interstitial nitrogen doping, it is proposed that the material obtained after 2 h of nitrogen plasma treatment is N-TiO_{2-x}/Pt.

The weight percentage of platinum and nitrogen in TiO_2, considering the XPS analysis, is presented in Table 1. The analysis was carried out on the signals corresponding to N

1s, as previously demonstrated while studying nitrogen-doped TiO_2. The energy binding value for N 1s was determined at 399.2 +/− 0.2 eV. A mathematical fitting was carried out for the N 1s signal in the HR-XPS spectrum for the nitrogen-doped TiO_2 compound, to calculate their related chemical content. The percentage of platinum metal and nitrogen increased in the samples when the time of plasma treatment increased up to 2 h, higher than those subjected to 1 h treatment. Therefore, the Pt and N content was about 80% and 24% higher, respectively, in comparison to that of the samples that underwent 1 h of plasma treatment. As confirmed by XPS analyses, the increase in both elements is proportional to the plasma processing time.

Table 1. Weight percent of Pt and N in N-TiO_{2-x}/Pt (XPS analysis).

Treatment Time (h)	% Weight	
	Pt	Nitrogen
1	1.6	0.38
2	2.9	0.47

3.4. Diffuse Reflectance Spectroscopy (DRS)

The reflectance and absorbance spectra of the metal-impregnated samples after 1 h and 2 h nitrogen of plasma treatments are presented in Figure 6. The diffuse reflectance UV–Vis spectra (DRS) for the standard (TiO_2 P25) and for the plasma-treated samples are shown in Figure 6a. The K/S relation that was obtained from the DRS data was determined by applying the Kubelka–Munk equation given by the following equation:

$$\frac{K}{S} = \frac{(1-R)^2}{2R} \quad (4)$$

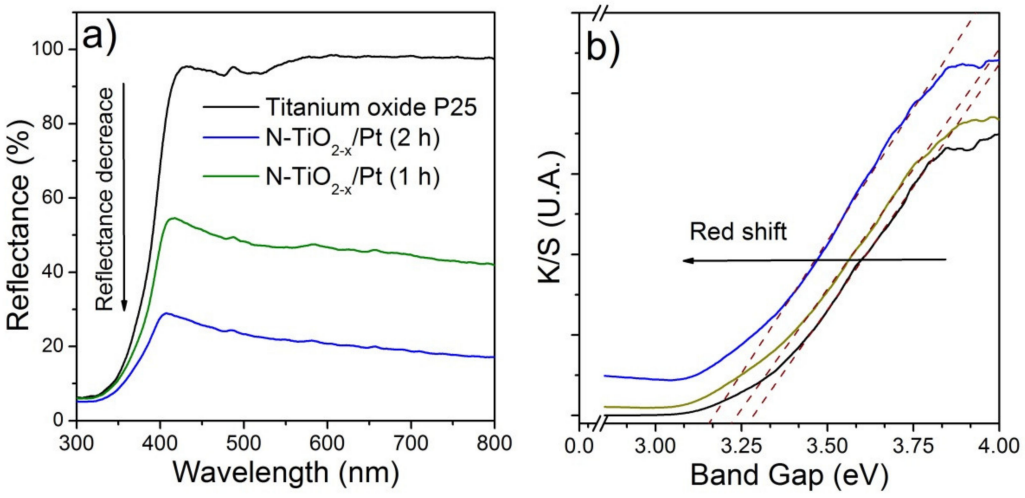

(**a**) (**b**)

Figure 6. (**a**) DRS spectra and (**b**) absorbance spectra after Pt impregnation in TiO_2.

The absorbance spectrum of the samples was obtained (Figure 6b), which allowed us to evaluate the band gap of each sample. The method is based on extrapolation of the straight line of the UV–Vis spectrum until it intersects with the x-axis of the wavelength or the band-gap energy (Figure 6). This wavelength intersection defines the band-gap energy for the semiconductor under consideration as $E_{bg} = hc/\lambda_{int}$.

Applying this method, one can observe that the nitrogen plasma treatment time is proportional to the incorporation or impregnation of platinum and nitrogen, which progressively reduces the bandwidth, as shown in Table 2. Therefore, one can conclude

that the absorption of photons is related to the impregnated or incorporated amount of Pt^0/nitrogen on the crystalline lattice of the sample's surface, resulting in lower energy absorption.

Table 2. Band gap of N-TiO_{2-x}/Pt samples considering different treatment times and 100 watts of power.

	P25	**TiO_2/Pt**	
Power		100 watts	
Time		1 h	2 h
Band Gap (eV)	3.28	3.23	3.17

3.5. High-Resolution Transmission Electron Microscopy (HRTEM)

HRTEM images of the samples are shown in Figure 7. The Pt nanoparticles were found successfully dispersed on the titanium oxide surface (Figure 7a). Therefore, a statistical analysis was performed by measuring the nanoparticles size from the HRTEM images. Thus, a histogram of the particle size distribution of Pt NPs in the N-TiO_{2-x}/Pt composite (Figure 7b) shows a narrow distribution in the range of 2–8 nm. Platinum NPs, with an average diameter of 5.0 nm, are well dispersed on the TiO_2 surface.

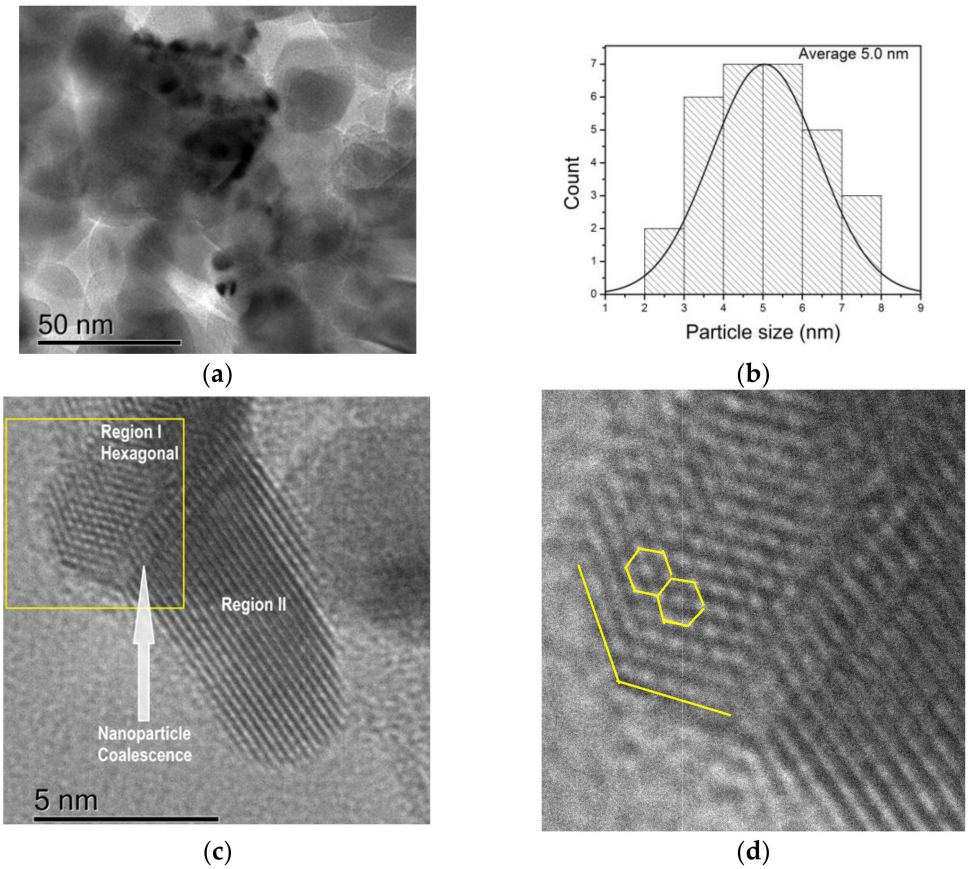

Figure 7. Transmission electron microscopy of platinum nanoparticles: (**a**,**b**) monodispersed platinum nanoparticles in the 2–8 nm range; (**c**) Pt nanoparticles in coalescence region; (**d**) zoom-in image of Figure 7c and the yellow square showing the boundaries.

HRTEM images reveal lattice fringe spacings corresponding to the Pt (111) plane. The interplanar spacing of the lattice fringes was 2.38 Å and 2.22 Å for Region I and Region II, respectively (Figure 7c). These results are consistent with the (111) d-spacing reported by others research groups for metallic Pt NPs [33,34]. It is noteworthy that we

observed two different crystalline patterns (Region I and Region II). Additionally, it can be seen that the boundary between these two regions (Figure 7c) is due to the coalescence induced by the crystallization of Pt nanoparticles. Grammatikopoulos et al. [35] applied classical molecular dynamics simulations to study the mechanisms driving the coalescence phenomena. They demonstrated that the driving force for the coalescence is due to the surface energy minimization associated with dangling bonds density and distribution. On the other hand, they also observed coalescence-assisted crystallization during the sintering of amorphous nanoparticles, reporting that the rotation started a seedless crystallization wave, which propagated through them, leading to near-perfect single or polycrystalline fcc structures.

Our hypothesis is that the mechanism described above is responsible for obtaining two platinum crystalline patterns. This nanoparticle was probably left in an intermediate crystallization state.

On the other hand, Figure 7d shows that the coalescence of a single Pt NPs, due to the plasma effect, has two different patterns: nano-hexagonal and fcc lattice fringes, suggesting that the nucleation of the hexagonal platinum crystal is along the [111] direction. Other researchers have reported having obtained similar symmetries in platinum, silver, and gold nanoparticles using chemical reduction procedures [34,36,37]. It is known that nucleation and growth are related to surface energy and growth rate, and their size depends on the growth rate and directions. The results obtained in the present work must be further studied to understand the crystallization process so as to be able to control the shape or size of the metallic nanoparticles by applying an energetic plasma to induce decorated specific surfaces.

4. Conclusions

The obtained N-TiO_{2-x}/Pt compound was successfully prepared by a novel nitrogen plasma method. After two hours of treatment, the crystal lattice and surface of TiO_2 contained up to 0.47% and 2.9% (wt%) of nitrogen and metallic platinum, respectively. Our results regarding the energy gap reveal that, under this method of synthesis, the band-gap value is reduced from 3.28 to 3.17 eV. These results demonstrate the effectiveness of the proposed methodology to carry out the simultaneous process of impregnating platinum metal particles on a titania surface and achieving nitrogen doping in a single step. Likewise, this method allows obtaining different patterns on a single metallic nanoparticle; therefore, the formation of a hexagonal shape opens a new window for the study of this phenomenon induced through plasma to obtain effective composite materials. In comparison to other used techniques to induce metal surface decoration, this method is environmentally safe, has low energy requirements, and can be carried out in a relatively short period time, representing a promising approach for the synthesis of N-TiO_{2-x}/Pt catalysts.

Author Contributions: Conceptualization, R.T.-T.; methodology, R.T.-T.; validation, P.Q.-O., R.R. and A.A.-O.; formal analysis, R.T.-T., P.Q.-O. and M.A.Á.-L.; investigation, R.T.-T.; data curation, R.T.-T.; writing—original draft preparation, R.T.-T.; writing—review and editing, P.Q.-O., R.R., A.A.-O., M.A.Á.-L. and R.T.-T.; supervision and project administration, R.T.-T. All authors have read and agreed to the published version of the manuscript.

Funding: This research received no external funding.

Acknowledgments: The authors would like to extend their deepest appreciation to CONACYT (Consejo Nacional de Ciencia y Tecnología) for the financial support of this research project under SEP-CONACYT no. 221418, FOMIX-Yucatan 2008-108160 and CONACYT LAB-2009-01 no. 123913, 188345, 204822, 292692, 294643, 299083, 300046 and 315860. HRTEM analyses were carried out in the Research Center in Applied Science and Technology of Tabasco, UJAT-DAIA (project 225962, CONCYT-INFRA 2014). The authors acknowledge D. Aguilar Treviño and W. Cauich of LANNBIO (CINVESTAV, Mérida) for the technical assistance in XRD and XPS determinations. The authors also thank S. García López for his support with TEM-SAED (Centro de Investigación en Ciencia y Tecnología Aplicada de Tabasco).

Conflicts of Interest: The authors declare no conflict of interest.

References

1. Fujishima, A.; Zhang, X.; Tryk, D.A. TiO_2 photocatalysis and related surface phenomena. *Surf. Sci. Rep.* **2008**, *63*, 515–582. [CrossRef]
2. Han, F.; Kambala, V.S.R.; Srinivasan, M.; Rajarathnam, D.; Naidu, R. Tailored titanium dioxide photocatalysts for the degradation of organic dyes in wastewater treatment: A review. *Appl. Catal. A Gen.* **2009**, *359*, 25–40. [CrossRef]
3. Wen, J.; Li, X.; Liu, W.; Fang, Y.; Xie, J.; Xu, Y. Photocatalysis fundamentals and surface modification of TiO_2 nanomaterials. *Chin. J. Catal.* **2015**, *36*, 2049–2070. [CrossRef]
4. Shen, R.; Xie, J.; Xiang, Q.; Chen, X.; Jiang, J.; Li, X. Ni-based photocatalytic H_2-production cocatalysts$_2$. *Chin. J. Catal.* **2019**, *40*, 240–288. [CrossRef]
5. Shen, J.; Wang, R.; Liu, Q.; Yang, X.; Tang, H.; Yang, J. Accelerating photocatalytic hydrogen evolution and pollutant degradation by coupling organic co-catalysts with TiO_2. *Chin. J. Catal.* **2019**, *40*, 380–389. [CrossRef]
6. Ikezawa, S.; Homyara, H.; Kubota, T.; Suzuki, R.; Koh, S.; Mutuga, F.; Yoshioka, T.; Nishiwaki, A.; Ninomiya, Y.; Takahashi, M.; et al. Applications of TiO_2 film for environmental purification deposited by controlled electron beam-excited plasma. *Thin Solid Films* **2001**, *386*, 173–176. [CrossRef]
7. Calza, P.; Minero, C.; Pelizzetti, A.E. Photocatalytic transformations of chlorinated methanes in the presence of electron and hole scavengers. *J. Chem. Soc. Faraday Trans.* **1997**, *93*, 3765–3771. [CrossRef]
8. Schmelling, D.C.; Gray, K.A.; Kamat, P. V The influence of solution matrix on the photocatalytic degradation of TNT in TiO_2 slurries. *Water Res.* **1997**, *31*, 1439–1447. [CrossRef]
9. Zallen, R.; Moret, M.P. The optical absorption edge of brookite TiO_2. *Solid State Commun.* **2006**, *137*, 154–157. [CrossRef]
10. Carp, O.; Huisman, C.L.; Reller, A. Photoinduced reactivity of titanium dioxide. *Prog. Solid State Chem.* **2004**, *32*, 33–177. [CrossRef]
11. Lee, D.-S.; Chen, Y.-W. Nano Ag/TiO_2 catalyst prepared by chemical deposition and its photocatalytic activity. *J. Taiwan Inst. Chem. Eng.* **2014**, *45*, 705–712. [CrossRef]
12. Rosu, M.; Socaci, C.; Floare-Avram, V.; Borodi, G.; Pogacean, F.; Coros, M.; Măgeruşan, L.; Pruneanu, S. Photocatalytic performance of graphene/TiO_2-Ag composites on amaranth dye degradation. *Mater. Chem. Phys.* **2016**, *179*, 232–241. [CrossRef]
13. Rosu, M.-C.; Coros, M.; Pogacean, F.; Magerusan, L.; Socaci, C.; Turza, A.; Pruneanu, S. Azo dyes degradation using TiO_2-Pt/graphene oxide and TiO_2-Pt/reduced graphene oxide photocatalysts under UV and natural sunlight irradiation. *Solid State Sci.* **2017**, *70*, 13–20. [CrossRef]
14. Zayadi, R.; Abu Bakar, F. Comparative study on the performance of Au/F-TiO_2 photocatalyst synthesized from Zamzam water and distilled water under blue light irradiation. *J. Photochem. Photobiol. A Chem.* **2017**, *346*, 338–350. [CrossRef]
15. Chiarello, G.L.; Dozzi, M.V.; Scavini, M.; Grunwaldt, J.-D.; Selli, E. One step flame-made fluorinated Pt/TiO_2 photocatalysts for hydrogen production. *Appl. Catal. B Environ.* **2014**, *160–161*, 144–151. [CrossRef]
16. Zielińska-Jurek, A.; Hupka, J. Preparation and characterization of Pt/Pd-modified titanium dioxide nanoparticles for visible light irradiation. *Catal. Today* **2014**, *230*, 181–187. [CrossRef]
17. Filippo, E.; Carlucci, C.; Capodilupo, A.L.; Perulli, P.; Conciauro, F.; Corrente, G.A.; Gigli, G.; Ciccarella, G. Enhanced photocatalytic activity of pure anatase TiO_2 and Pt-TiO_2 nanoparticles synthesized by green microwave assisted route. *Mater. Res.* **2015**, *18*, 473–481. [CrossRef]
18. Zhu, X.; Cheng, B.; Yu, J.; Ho, W. Halogen poisoning effect of Pt-TiO_2 for formaldehyde catalytic oxidation performance at room temperature. *Appl. Surf. Sci.* **2016**, *364*, 808–814. [CrossRef]
19. Jedsukontorn, T.; Saito, N.; Hunsom, M. Photocatalytic behavior of metal-decorated TiO_2 and their catalytic activity for transformation of glycerol to value added compounds. *Mol. Catal.* **2017**, *432*, 160–171. [CrossRef]
20. Giannakas, A.E.; Antonopoulou, M.; Papavasiliou, J.; Deligiannakis, Y.; Konstantinou, I. Photocatalytic performance of Pt-TiO_2, Pt-N-TiO_2 and Pt-N/F-TiO_2 towards simultaneous Cr(VI) reduction/benzoic acid oxidation: Insights into photogenerated charge carrier dynamics and catalyst properties. *J. Photochem. Photobiol. A Chem.* **2017**, *349*, 25–35. [CrossRef]
21. Sui, Y.; Liu, S.; Li, T.; Liu, Q.; Jiang, T.; Guo, Y.; Luo, J.-L. Atomically dispersed Pt on specific TiO_2 facets for photocatalytic H2 evolution. *J. Catal.* **2017**, *353*, 250–255. [CrossRef]
22. Trejo-Tzab, R.; Alvarado-Gil, J.J.; Quintana, P. Photocatalytic activity of Degussa P25 TiO_2/Au obtained using Argon (Ar) and Nitrogen (N2) plasma. *Top. Catal.* **2011**, *54*, 250–256. [CrossRef]
23. Trejo-Tzab, R.; Alvarado-Gil, J.J.; Quintana, P.; Bartolo-Pérez, P. N-doped TiO_2 P25/Cu powder obtained using nitrogen (N2) gas plasma. *Catal. Today* **2012**, *193*, 179–185. [CrossRef]
24. Trejo-Tzab, R.; Caballero-Espada, L.; Quintana, P.; Ávila-Ortega, A.; Medina-Esquivel, R.A. Controlled Phase Changes of Titania Using Nitrogen Plasma. *Nanoscale Res. Lett.* **2017**, *12*, 32. [CrossRef]
25. Qayyum, A.; Zeb, S.; Ali, S.; Waheed, A.; Zakaullah, M. Optical emission spectroscopy of abnormal glow region in nitrogen plasma. *Plasma Chem. Plasma Process.* **2005**, *25*, 551–564. [CrossRef]
26. Abdel-Fattah, E.; Bazavan, M.; Sugai, H. Langmuir probe diagnostics of electron energy distributions with optical emission spectroscopy in capacitively coupled rf discharge in nitrogen. *J. Appl. Phys.* **2011**, *110*, 113303. [CrossRef]

27. Spurr, R.A.; Myers, H. Quantitative Analysis of Anatase-Rutile Mixtures with an X-Ray Diffractometer. *Anal. Chem.* **1957**, *29*, 760–762. [CrossRef]
28. Ihnatiuk, D.; Tossi, C.; Tittonen, I.; Linnik, O. Effect of Synthesis Conditions of Nitrogen and Platinum Co-Doped Titania Films on the Photocatalytic Performance under Simulated Solar Light. *Catalysts* **2020**, *10*, 1074. [CrossRef]
29. Naitabdi, A.; Boucly, A.; Rochet, F.; Fagiewicz, R.; Olivieri, G.; Bournel, F.; Benbalagh, R.; Sirotti, F.; Gallet, J.-J. CO oxidation activity of Pt, Zn and ZnPt nanocatalysts: A comparative study by in situ near-ambient pressure X-ray photoelectron spectroscopy. *Nanoscale* **2018**, *10*, 6566–6580. [CrossRef]
30. Matin, A.; Lee, E.; Kim, H.; Yoon, W.; Kwon, Y. Rational syntheses of core–shell Fe@(PtRu) nanoparticle electrocatalysts for the methanol oxidation reaction with complete suppression of CO-poisoning and highly enhanced activity. *J. Mater. Chem. A* **2015**, *3*, 17154. [CrossRef]
31. Viswanathan, B.; Krishanmurthy, K.R. Nitrogen Incorporation in TiO_2: Does It Make a Visible Light Photo-Active Material? *Int. J. Photoenergy* **2012**, *2012*, 269654. [CrossRef]
32. Di Valentin, C.; Finazzi, E.; Pacchioni, G.; Selloni, A.; Livraghi, S.; Paganini, M.C.; Giamello, E. N-doped TiO_2: Theory and experiment. *Chem. Phys.* **2007**, *339*, 44–56. [CrossRef]
33. Michel, J.A.; Morris, W.H.; Lukehart, C.M. Synthesis of shaped Pt nanoparticles using common anions or small molecules as shape-directing agents: Observation of a strong halide or pseudo-halide effect. *J. Mater. Chem. A* **2015**, *3*, 2012–2018. [CrossRef]
34. Ha, H.-W.; Kim, I.Y.; Hwang, S.-J.; Ruoff, R.S. One-Pot Synthesis of Platinum Nanoparticles Embedded on Reduced Graphene Oxide for Oxygen Reduction in Methanol Fuel Cells. *Electrochem. Solid-State Lett.* **2011**, *14*, B70. [CrossRef]
35. Grammatikopoulos, P.; Cassidy, C.; Singh, V.; Sowwan, M. Coalescence-induced crystallisation wave in Pd nanoparticles. *Sci. Rep.* **2015**, *4*, 5779. [CrossRef] [PubMed]
36. Rodríguez-León, E.; Iñiguez-Palomares, R.; Navarro, R.E.; Herrera-Urbina, R.; Tánori, J.; Iñiguez-Palomares, C.; Maldonado, A. Synthesis of silver nanoparticles using reducing agents obtained from natural sources (Rumex hymenosepalus extracts). *Nanoscale Res. Lett.* **2013**, *8*, 318. [CrossRef]
37. Hu, J.; Wang, Z.; Li, J. Gold Nanoparticles With Special Shapes: Controlled Synthesis, Surface-enhanced Raman Scattering, and The Application in Biodetection. *Sensors* **2007**, *7*, 3299–3311. [CrossRef]